processes

MDPI

Article

Investigation of the Mixing Time Distribution and Connected Flow Fields in Two-Stage Stirred Vessels

Marian Matzke [1,2,3], Mathias Ulbricht [3] and Heyko Jürgen Schultz [1,2,*]

[1] Department of Chemical Engineering, Faculty of Chemistry, University of Applied Sciences Niederrhein, Adlerstraße 32, 47798 Krefeld, Germany
[2] Institute for Coating and Surface Chemistry (ILOC), University of Applied Sciences Niederrhein, Adlerstraße 32, 47798 Krefeld, Germany
[3] Department of Technical Chemistry II, Faculty of Chemistry, University of Duisburg-Essen, Universitätsstraße 7, 45141 Essen, Germany; mathias.ulbricht@uni-essen.de
* Correspondence: heyko_juergen.schultz@hs-niederrhein.de

Abstract: In this study, laser-induced fluorescence is used to investigate the homogenization in stirred vessels equipped with single- and two-stage stirrers. The acquired local mixing times across the reactor cross-section are plotted as mixing time distribution (MTD) and then compared with the previously measured flow fields of the identical systems. With the help of a novel evaluation method, the mixing times are characterized with a normal distribution fit. With mean value and standard deviation as determined parameters, the mixing results of different installation heights and stirrer combinations are quantitatively evaluated and lead to clear recommendations for installations that enable efficient mixing.

Keywords: two-stage impellers; stirred vessels; laser-induced fluorescence (LIF); mixing time; flow fields

Citation: Matzke, M.; Ulbricht, M.; Schultz, H.J. Investigation of the Mixing Time Distribution and Connected Flow Fields in Two-Stage Stirred Vessels. *Processes* **2024**, *12*, 132. https://doi.org/10.3390/pr12010132

Academic Editor: Farhad Ein-Mozaffari

Received: 12 December 2023
Revised: 29 December 2023
Accepted: 2 January 2024
Published: 4 January 2024

1. Introduction

The mixing time is a quantity, which is often used for the assessment of the efficiency of the blending process inside chemical reactors. Most of the established experimental methods for the measurement of mixing time, however, are incapable of describing the mixing process in its entirety. The common decolorization method, for instance, which uses an acid–base reaction with a color change upon pH change, usually only focuses on the point in time when the entire liquid volume is mixed and the color change is completed ("global mixing time") [1,2]. For an efficient mixing process with minimal energy requirements, however, the aim should be to provide the desired degree of mixing at the same time throughout the entire volume, which the classic measurements methods cannot assess. Therefore, this study presents the attempt of a novel method of assessing the mixing process, with the aim of establishing design recommendations for energy-efficient stirred tank reactors.

Laser-induced fluorescence (LIF) is a non-invasive, laser-optical measurement technique to detect local concentration, temperature or pH value, simultaneously at multiple locations in a laser light sheet [1,3–6]. A fluorescent dye, such as fluorescein or rhodamine, is used as a tracer. This dye absorbs the incoming laser light and subsequently emits fluorescence light with a different wavelength. With the aid of suitable optical filters, the wavelength of the laser light can be filtered, so that only the fluorescence is captured using a camera.

The intensity of the emitted fluorescence I_F is proportional to the amount of absorbed light I, which is calculated according to Lambert–Beer's law, using the intensity of the incoming light I_0, the molar extinction coefficient ε, and the absorption path length b. Φ is

the quantum efficiency of the respective dye and serves as the proportionality factor (see Equation (1)):

$$I_F = \Phi \cdot I = \Phi \cdot I_0 \cdot e^{-\varepsilon \cdot b \cdot c} \quad (1)$$

In a certain range of relatively low concentrations c, it is valid to simplify this equation into Equation (2), resulting in a linear relation between concentration and fluorescence intensity, with K as a measurement system-dependent constant [1]:

$$I_F = \Phi \cdot I_0 \cdot K \cdot \varepsilon \cdot b \cdot c \quad (2)$$

Consequently, the target quantity, in this case the local dye concentration, can be calculated directly from the image brightness, provided that the experiment is conducted within this range of linearity. The LIF is an established measurement method that has been used in several studies concerning mixing processes in stirred tank reactors, investigating the influence of the position of tracer addition [7], the mixing process in connection to chemical reactions [8–10], different impeller types [11,12] as well as mixing in a continuously operated tank [13].

In previous studies, concentration data were often extracted only at a finite number of locations within the vessel, not fully utilizing the potential of the LIF as a whole field technique. Stefan et al. [4,14], for example, used six defined locations, whereas Distelhoff et al. [15] used eight locations to determine the mixing time for a variety of impeller types. In contrast to that, the experimental setup used in this study is capable of determining the local mixing times for the entire cross-section of the reactor. The evaluation concept used in this study is based on Bliem's work [4], who developed a MATLAB code to obtain local mixing times across the entire cross-section of the vessel, as well as Stefan et al.'s study [14], which included the first iteration of a Visual Basic evaluation. This concept is further expanded here, by describing the distribution of the local mixing times as a mathematical function.

The second main difference between this study and the majority of investigations found in the literature is the tracer addition, which usually takes place at the liquid surface [16–19]. Here, the dye enters the system via a custom 3D-printed injection baffle. This element was primarily developed for flow field investigations with the fluorescence tracer method [20], which required a reproducible tracer addition in close proximity of the impeller.

Third, this study also takes the flow fields of the investigated impeller setups into account, which were obtained in previous studies using stereo particle image velocimetry [21,22]. This facilitates the identification and description of the relationships between the flow patterns and the mixing process. By additionally introducing a mathematical description of the mixing time distribution, the aim of this study is to describe the mixing process holistically.

2. Materials and Methods

2.1. Setup

Experiments were conducted in the same laser-optical testing facility that was used to investigate flow patterns in stirred tanks [21–23] as well as other processes [24] during previous studies from this workgroup.

For LIF measurements, the reactor is placed inside an outer tank of polyhedral shape, which is also used for stereo particle image velocimetry (PIV) measurements [21,22]. It is filled with tap water in order to minimize light refraction at the cylindrical tank's surface. A continuous wave (CW) laser, which emits green light with a wavelength of 532 nm, is used for illumination. With a light sheet optics device attached, the laser light is expanded to a light sheet plane. The laser sheet enters the tank from the side and is positioned at the central plane of the reactor. As a consequence, only one half of the tank can be analyzed with this setup, since the impeller(s) and the shaft cast a shadow on the opposite half (cf. Figure 1).

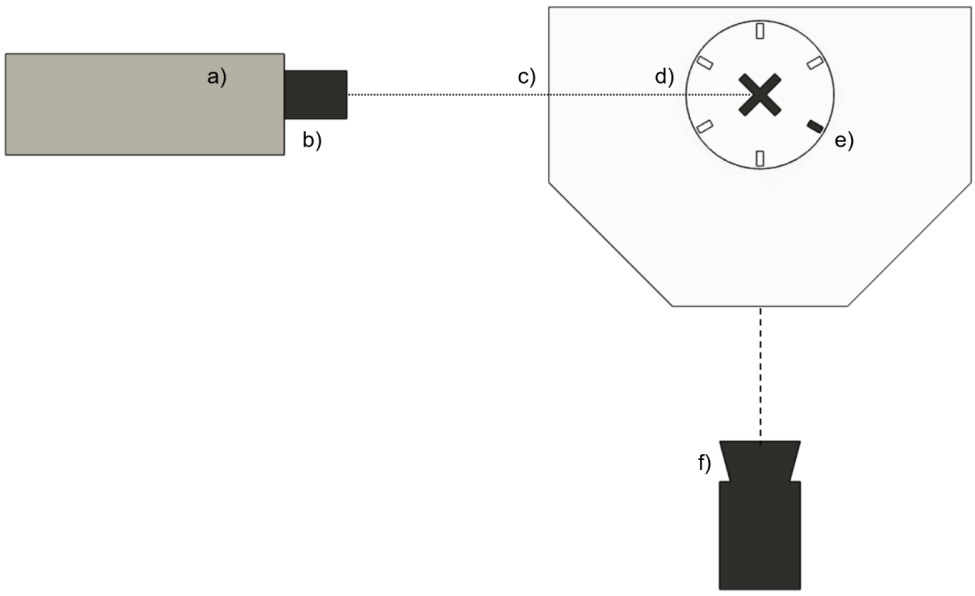

Figure 1. LIF setup, top view. (**a**) CW laser. (**b**) Light sheet optics. (**c**) Polyhedral aquarium. (**d**) Vessel with stirrers and internals. (**e**) 3D-printed injection baffle. (**f**) CCD camera. The dotted line represents the position of the laser light sheet.

Images are acquired with a "FlowSense EO 4M" CCD camera, supplied by Dantec Dynamics, Denmark, with a resolution of 2048 × 2048 pixels. It is set up in front of the reactor and therefore in a 90° angle to the laser light sheet. While this type of camera is also capable of acquiring double-frame images within a short timeframe, which is used for PIV measurements, it is set to the single-frame mode for this study. In order to detect the fluorescence intensity with a sufficiently high resolution, 12-bit images with a total of 4096 (=2^{12}) grayscale levels are used instead of the 8-bit images that are usually suitable for PIV measurements [21,22]. The camera is equipped with an optical filter module that is only transparent for light with wavelengths $\lambda \geq 550$ nm. Due to that, only the fluorescence light is captured within the acquired images while the laser light is blocked. Compared to PIV measurements, the laser is operated with an approximately 2.5 times higher energy output [4,25].

The geometric features of tank, baffles and impellers are also mostly identical to those used in previous studies from this workgroup [20,22]. A PMMA vessel with an inner diameter of 110 mm is equipped with a set of six rectangular baffles with a width of 11 mm (d_B = D/10), positioned at a distance to the wall of 2.2 mm (=D/50). In the reference experiments, impellers with a standard diameter ratio d/D of 1/3 [5] are used, which is also most commonly investigated in the literature. The combinations of different impeller types consist of a Rushton turbine with a diameter of 0.28 D and a pitched blade turbine with 0.35 D. As determined via torque measurements, both of these impellers exhibit an identical power input, when operated individually [22]. With the exception of the specific impeller diameters and the number of baffles, this setup is in accordance with recommendations found in the literature [1,2,5,26,27].

An increased number of baffles is unavoidable for laser-optical measurements in multi-stage stirring processes in order to minimize surface motion and gas intake [20]. This is especially relevant in the fully turbulent flow regime, since light reflections at the curved liquid surface can damage the utilized CCD camera [21,25]. In order to further minimize the impact of surface motion, a ring is 3D-printed out of flexible thermoplastic polyurethane (TPU) material and attached to the outside of the reactor. A small layer of the moving liquid surface is therefore intentionally covered, masking this region within the resulting images. As a consequence, the plots displayed in the results section do not extend over the entire filling height; but with less than 2% of the cross-section area, the

corresponding information loss is minimal and can therefore be neglected. A secondary ring covers the adhesive seam between the reactor bottom and the cylindrical corpus (cf. Figure 2).

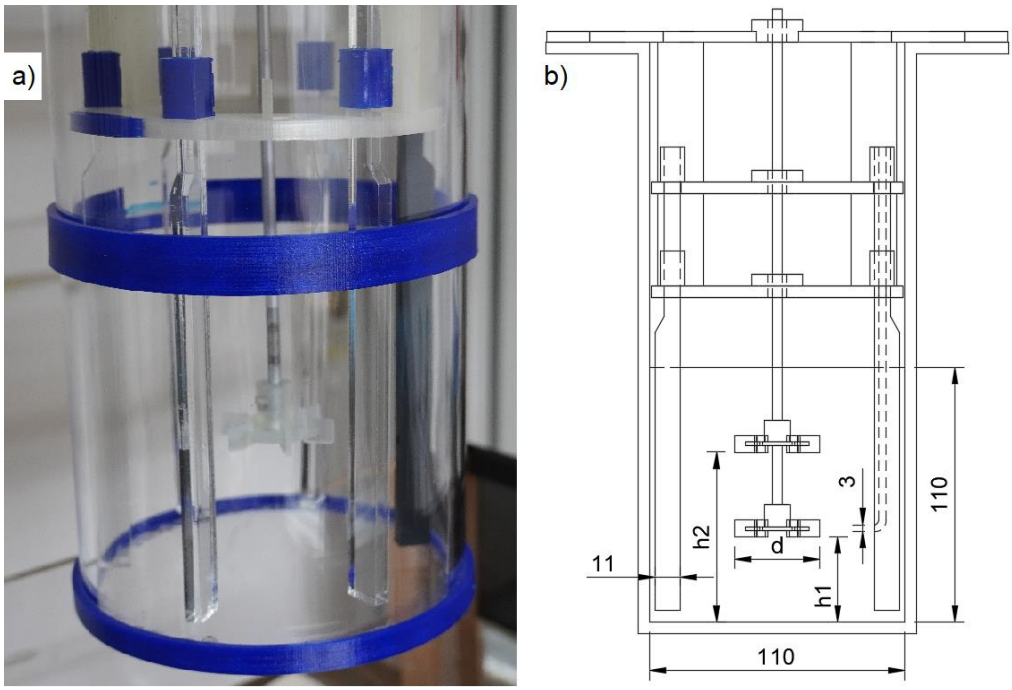

Figure 2. (**a**) Baffled PMMA reactor, with injection baffle (black). (**b**) Schematic drawing of the reactor geometry, dimensions given in (mm).

2.2. Calibration

As a first step of LIF measurements, a calibration procedure is performed in order to identify the range of dye concentration where the linear correlation to fluorescence intensity applies. For that purpose, different concentrations of dye are successively set inside the reactor. It is practical to measure the lowest selected concentration first and add small volumes of dye solution over the course of the calibration [14,25]. After each injection, the liquid is mixed under turbulent conditions for about two minutes until a steady state is reached. Afterward, with the laser activated, a set of 50 images is acquired using the camera. In the Dynamic Studio database, the respective dye concentration inside the reactor is manually assigned to the dataset. Once all specified concentrations are measured and the corresponding images are saved in the database, the calibration takes place, connecting the brightness of the images to the specified dye concentration. This is performed for each individual pixel. Therefore, care must be taken to ensure that any involved part of the setup is positioned at the same location during the entire calibration as well as for all subsequent measurements. If this is the case, the baffles and/or internals are considered as background objects and do not influence the conversion of image brightness into concentration. During the subsequent measurements, minor positional deviations in the magnitude of up to 1 mm are unavoidable, but are acceptable due to the division of the image into a grid, as described in Section 2.4 [28].

With the average brightness across each set of images, the calibration function displayed in Figure 3 is created. Within the concentration range from 0 to 140 µg/L, the linear correlation between fluorescence intensity and concentration can be identified. Therefore, LIF experiments are conducted with a significantly lower dye concentration than the fluorescence tracer method, which was performed with the same substances [20,29].

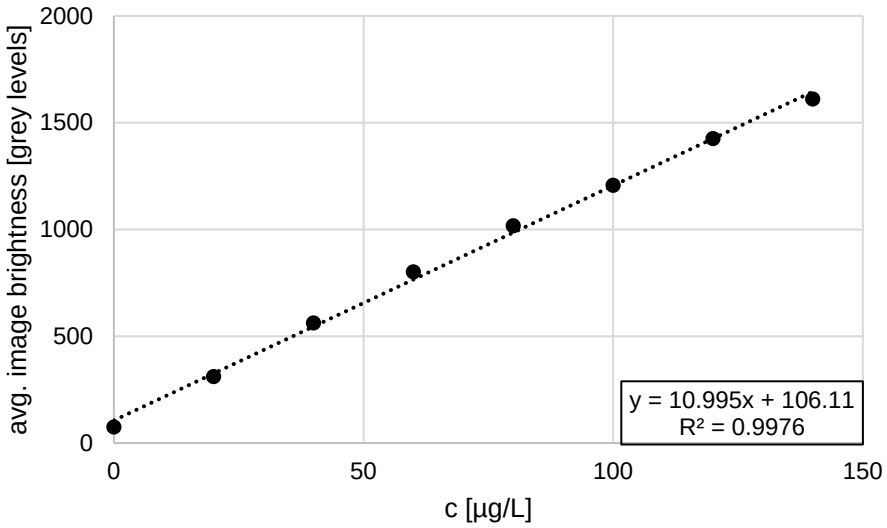

Figure 3. LIF calibration function, acquired via Dynamic Studio.

2.3. Measurements

For measurements, the tank is filled with tap water to a level of 110 mm (therefore H/D = 1). The impeller and internals are positioned and the stirrer motor is activated at the respective rotational frequency. In contrast to PIV measurements, the usage of a refractive index matching (RIM) fluid [21,23] is not suitable for mixing experiments, because the fluid has to be replaced after every measurement. As a consequence, the inserted baffles are visible within the acquired images. With the previous calibration, however, the evaluation is feasible with only minor measurement errors in the baffle region, due to one baffle edge being visible in the acquired images. This must be taken into account when interpreting the following figures, where the baffle is observable by a slight vertical stripe in a negligibly small area of the figures.

Once the flow reaches a stationary state, the laser and the camera are activated and 1 mL of a Rhodamine B solution with a concentration of 90 mg/L is inserted into the system via the injection baffle displayed in Figure 2b. This ensures a reproducible tracer injection at 1/3 of the filling height H [20]. Upon completed mixing, a concentration of approximately 90 µg/L is present in the reactor volume, which lies within the previously determined calibration interval of linearity (cf. Figure 3).

Similar to PIV measurements, the camera is synchronized with the impeller and acquires one image upon each completed impeller rotation. This is achieved using an "ROS" optical sensor by Monarch Instruments, which is oriented at a reflective element on the rotating stirrer shaft. As a consequence, the impeller position is identical in each individual image. The image acquisition is initiated before the dye injection and ends at least 50 impeller rotations after the image brightness on the monitor is deemed constant, which indicates that the mixing process is completed. Therefore, the acquired sequences of images vary in length, according to the respective experimental conditions. After the image acquisition is finished, the laser and impeller are deactivated. The reactor and internals are removed from the measurement construction, emptied, rinsed and reinserted afterward.

2.4. Evaluation

With the aid of the previously obtained linear calibration function, the image brightness can be converted into local concentration values via the "LIF Processing" algorithm in the Dynamic Studio software [30]. Additionally, areas outside of the reactor are masked and thereby blacked out. In order to evaluate the mixing time from these processed image sequences, the numeric concentration data as well as the timestamps of the images are exported and further processed using a Visual Basic algorithm [14]. Although it would be possible to extract the temporal course of concentration for every single pixel of the images,

the area was divided by a grid in order to accelerate the evaluation process. A region size of 16 × 16 pixel was chosen in analogy to the common interrogation area dimensions for PIV measurements [31]. For each region, a concentration–time (c–t) curve is extracted [4].

The point in time when the dye enters the system, and therefore the brightness begins to increase, is defined as t = 0 [25]. For each of the curves, the final dye concentration is determined by averaging the values of the last 20 images. Furthermore, an interval with respect to the specified mixing quality is created. In this case, for a mixing quality of 95%, this interval extends between 95 and 105% of the previously determined final dye concentration [14]. Afterward, the algorithm begins at the last timestamp and moves backward in time, until the c–t curve leaves the mixing quality interval for the first time. This specific timestamp is marked as the local mixing time t_M for the respective region [14]. With the individual mixing times for all regions, the mixing time distribution (MTD) can be obtained and displayed as a contour plot [4].

With this approach, it is possible to achieve reproducible results, as exemplarily shown in Figure 4, which presents the great conformity of four exemplary repeated measurements. However, during this study, this could not be achieved for all investigated setups, despite conducting at least three experiments each. Therefore, a complete statistical evaluation of the MTD is not feasible within the scope of this study.

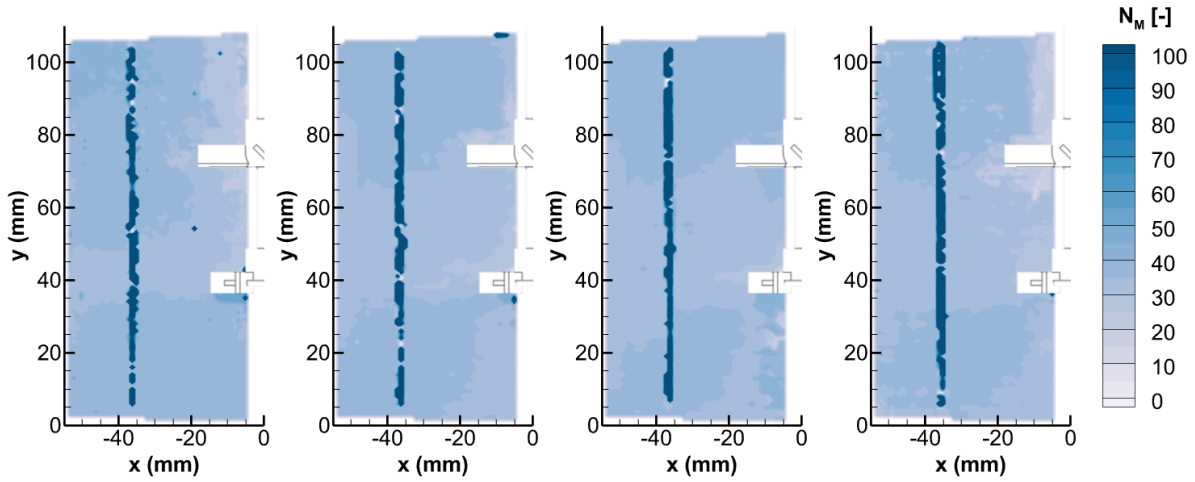

Figure 4. MTD plots resulting from the repeated measurements of the RT + PBT impeller combination, $h_1/D = 1/3$, $h_2/D = 2/3$, at $Re_R = 10{,}000$.

3. Results

Throughout Section 3, the MTD plots for the different investigated impeller setups are presented, with the local mixing time indicated by the coloring scheme (left part of the x–y plot in the figures). In this context, light shades represent shorter local mixing times while dark shades represent longer local mixing times within the respective left sections of the plots. These mixing times t_M are multiplied with the respective rotational frequencies n and are thus displayed in the dimensionless notion, according to Equation (3):

$$N_M = t_M \cdot n \quad (3)$$

Essentially, this quantity represents the number of impeller rotations that are necessary to reach the required level of homogeneity (here: 95 %) [2] and allows for a comparison of results between different measurements as well as with the literature data.

For reference, the PIV-derived flow fields of the investigated impellers and combinations, which were investigated in the aforementioned previous studies [21,22], are discussed in connection to the MTD plots. The flow fields are displayed in the right part of the x–y plots in the figures, with the light shades in this region indicating high flow velocity, and darker shades indicating low flow velocity.

Due to the usage of different fluids (LIF: tap water; PIV: aqueous ammonium thiocyanate solution), the two measurements were conducted with different rotational frequencies that led to the same Reynolds number of 10,000. For the same reason, all of the MTD plots presented in this section contain a vertical shading in the region around x = −37 mm. This is caused by a visible baffle edge and is therefore considered an optical artifact that is not taken into account for the evaluation of the results. These acrylic glass elements are made invisible in the PIV images through the RIM technique.

The third segment of the figures contains a graphical representation of the mixing time distribution. The experimentally determined local mixing times are divided into classes with a width ΔN_M of 5 and displayed as a bar chart, representing the distribution density. In addition to that, a normal distribution fit is applied to these data via the least squares method. The resulting cumulative distribution function is represented as a dashed line, applied to the secondary vertical axis. Since the aforementioned baffle region contains less than 100 of the approx. 5000 data points, the effect on the distribution functions is negligible. The respective fit parameters of these functions, i.e., the mean value μ and the standard deviation σ, are summarized in Table 1. Additionally, the literature values are included in the sub-sections for the purpose of comparison, if available for the respective impeller setup. As some of these values are based on a different level of homogeneity than the 95% used here, they are recalculated with Equation (4) [4,32]:

$$t_{M,95\%} = t_{M,\alpha\%} \cdot \frac{\ln\left(1 - \frac{95}{100}\right)}{\ln\left(1 - \frac{\alpha}{100}\right)} \quad (4)$$

Table 1. Overview of determined distribution parameters. Values in italics mark the experiment affected by laser-light fluctuations. Values in bold indicate the respective lowest mean and standard deviation.

	Single Stage		**1/4 + 3/4**		**1/3 + 2/3**		**5/12 + 7/12**	
	μ	**σ**	**μ**	**σ**	**μ**	**σ**	**μ**	**σ**
RT	42.5	5.4	44.1	9.7	27.5	5.8	35.9	3.2
PBT	54.4	9.9	31.7	3.2	**24.7**	5.2	40.7	4.4
RT + PBT	N/A		30.8	3.5	35.3	**2.8**	*34.5*	*6.0*
PBT + RT	N/A		49.6	9.7	53.1	8.3	41.1	5.0

3.1. Single-Stage Impellers

First, the results of single-stage reference experiments are presented and discussed, featuring a radially conducting Rushton turbine and an axially conducting pitched blade turbine. These impellers with a standard diameter of D/3 were positioned at the standard installation height of H/3.

The MTD plot for the Rushton turbine on the left of Figure 5a reveals a comparatively uniform mixing time distribution, with the lowest values found directly in the region of the radial impeller discharge stream. On the one hand, this observation fits well with the theory and, on the other hand, also very well with the flow field, which can be seen on the right of Figure 5a. Between the two ring vortices, the radial discharge stream forms the zone with the greatest flow velocity and turbulence. The shortest mixing time can also be observed in this region, which indicates intensive mixing in the main radial discharge flow. The dimensions of the two vortices, described and derived by the main flow vectors, are around (0.75–0.9) d, with the lower ring vortex, limited by the vessel walls, appearing somewhat smaller than the upper one. At the bottom of the vessel, in the vicinity of the walls, below the level line and in the core of the ring vortices, slightly longer mixing times can be seen, in line with the lower flow velocity there. Nevertheless, the mixing time distribution displayed in Figure 5b shows a satisfactory similarity and therefore a quite uniform distribution over the entire volume, resulting in a mean value μ = 42.5 for the dimensionless mixing time with a corresponding standard deviation of 5.4. In Distelhoff et al.'s study [15], a value of 37.1 can be found for this system, which

is slightly lower, but in the same order of magnitude as these results. This deviation can be explained by the higher impeller Reynolds number of 24,000 used during their measurements.

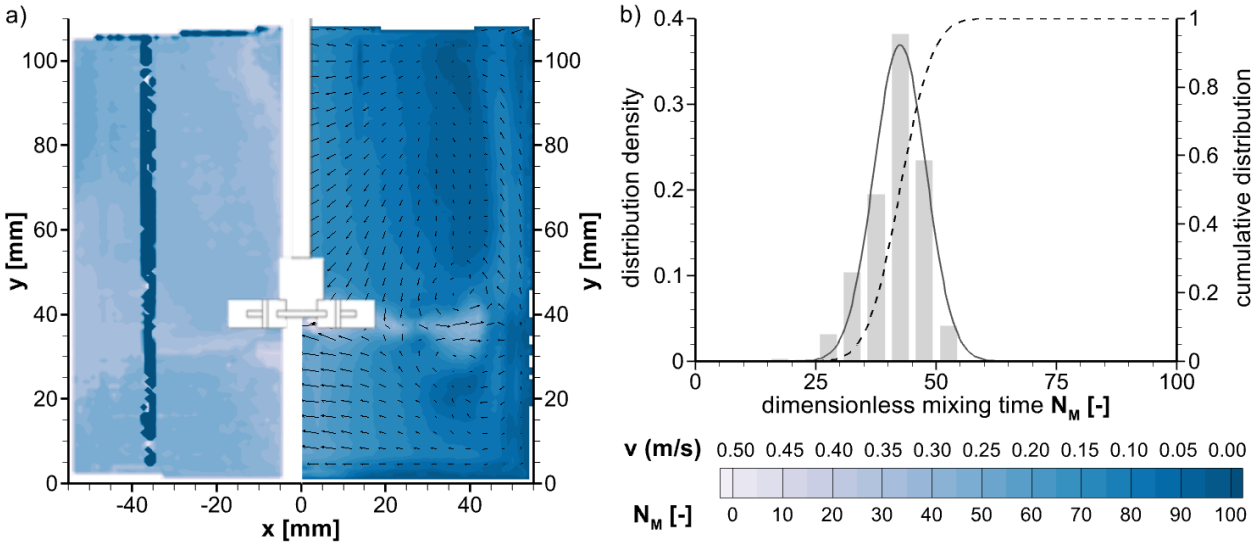

Figure 5. (**a**) MTD plot (left) and flow field (right) of the single-stage Rushton turbine at Re_R = 10,000. (**b**) Distribution density (solid line) and cumulative distribution (dotted line) of the corresponding dimensionless mixing time.

For the pitched blade turbine in Figure 6a, it is evident that the fastest mixing times can be found in the lower regions of the reactor, close to the main axial circulation. This observation again fits very well with the velocity profile that can be seen in the image on the right. The axial main flow, which is initially directed downward, appears to change direction at 10–15% of the filling level and to be deflected upward. Low flow velocity is found in the upper 30–40% of the filling level, with the axial ring vortex leading back to the suction side of the agitator at about 65% of the filling level. The vortex thus has an approximate dimension of 1.25 d. In contrast to the radial ring vortices, the core of the axial vortex seems to be mixed more intensively, which is why the mixing times are short here, especially on the suction side of the stirrer. As is to be expected, the regions close to the vessel walls and the vessel bottom, but especially just below the filling level line near the surface, are again mixed rather poorly, which leads to long mixing times here. Slow mixing correlates with exceptionally low flow velocity. Compared to the radial agitator, the mixing time distribution over the entire volume is not as homogeneous and uniform as for the axial agitator setup and results in a wider distribution (see Figure 6b). This leads to a mean value μ = 54.4 for the dimensionless mixing time that is 28% higher than the value for the Rushton turbine and a nearly doubled corresponding standard deviation of 9.9 (+83%). In this case, the difference between the mixing time and the literature value of 33.8 [15] is significantly larger than for the Rushton turbine.

While the single Rushton turbine already provides a satisfactory mixing performance at Re_R = 10,000, the results indicate that the single-stage pitched blade turbine was not operated with ideal parameters. Higher Reynolds numbers are probably necessary to avoid inhomogeneous and nonuniform mixing, which can also lead to disadvantages when implemented for technical processes.

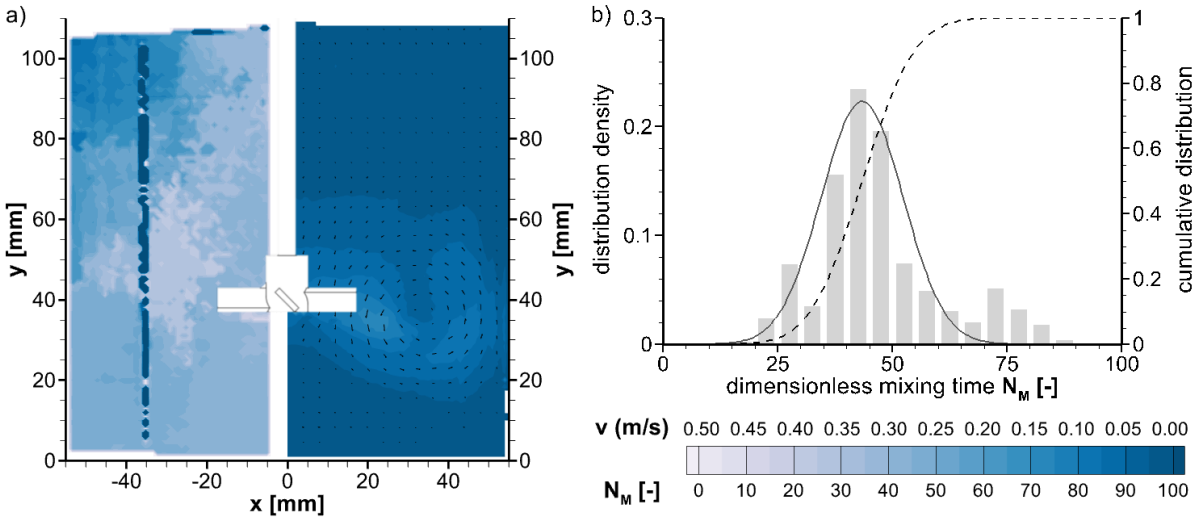

Figure 6. (**a**) MTD plot (left) and flow field (right) of the single-stage pitched blade turbine at Re_R = 10,000. (**b**) Distribution density (solid line) and cumulative distribution (dotted line) of the corresponding dimensionless mixing time.

3.2. Combinations of Identical Impellers

For the second set of experiments, impeller combinations of either two Rushton turbines or two pitched blade turbines were installed. In these cases, it is known that the impeller installation heights and the distance between individual stages provide a significant impact on the resulting flow conditions [20,33–39].

In the large distance scenario of the two-stage Rushton turbine in Figure 7a ($h_1/D = 1/4$, $h_2/D = 3/4$), the "parallel flow" pattern [35] can be clearly identified by the flow field on the right side. The two impellers operate mostly independently, resulting in two individual radial circulations with their four specific ring vortices in the respective compartments, each occupying approximately half of the reactor height. As a consequence, the primary mixing zone with the shortest local mixing times, visible on the left side of Figure 6a, is formed by the inward-oriented backstreams of the two circulations, which merge in the boundary region of the two compartments. This finding indicates that not only is high flow velocity alone responsible for short mixing times, but also turbulence, which, in our study, is caused by the two middle colliding ring vortices (the upper vortex from the lower stage and the lower one from the upper stirrer stage) both returning to the suction side of their particular stirrer stages. The MTD data in Figure 7b show that this configuration does not provide any advantage compared to the single-stage Rushton turbine (cf. Figure 5), as both the mean mixing time and the standard deviation are slightly higher (μ = 44.1, σ = 9.7).

With the turbines positioned at the standard installation heights ($h_1/D = 1/3$, $h_2/D = 2/3$; see Figure 8a) or even closer toward each other ($h_1/D = 5/12$, $h_2/D = 7/12$; see Figure 9a), the "merging flow" pattern [35] is formed, a singular intensive radial flow field that encompasses the entirety of the volume, as can be seen on the right side of the figures. The respective MTD plots on the left side of the figure shows shorter mixing times everywhere in the volume, with a more uniform distribution. However, low values in the combined main discharge flow, in the middle between the two stirrer stages, in particular once again indicate the influence of turbulence and not only absolute flow velocity on mixing times. From Figures 7b and 8b, it can be derived that both configurations with the smaller stage distance deliver lower mean dimensionless mixing times with μ = 27.5 and μ = 35.9, respectively. At σ = 5.8 and σ = 3.2, the standard deviation is lower or in the same order of magnitude as for the single stage (cf. Figure 5), but significantly lower than for the two-stage version with a large distance (cf. Figure 7). These results are in line with Rutherford et al. [35], who also found lower mixing times with the standard setup and the "merging flow" pattern, compared to the increased distance and the "parallel flow". The observed

difference of about 38% found in this study is slightly higher than the 20% from the literature, which can again be explained by the different investigated Reynolds numbers.

In comparison to the single-stage variant (cf. Figure 5), the two-stage variant of the radially conveying Rushton turbine exhibits a shorter and comparable or more homogeneous mixing time across the volume. This was expected, as the "merging flow" pattern can be observed in these two presented height constellations (Figures 8 and 9). In contrast, the large distance constellation with the "parallel flow" pattern [35] even leads to worse mixing times and standard deviations (cf. Figure 7). Considering that the second impeller would also double the power input without advantages regarding mixing times in this case [40], this impeller setup cannot be recommended for mixing processes.

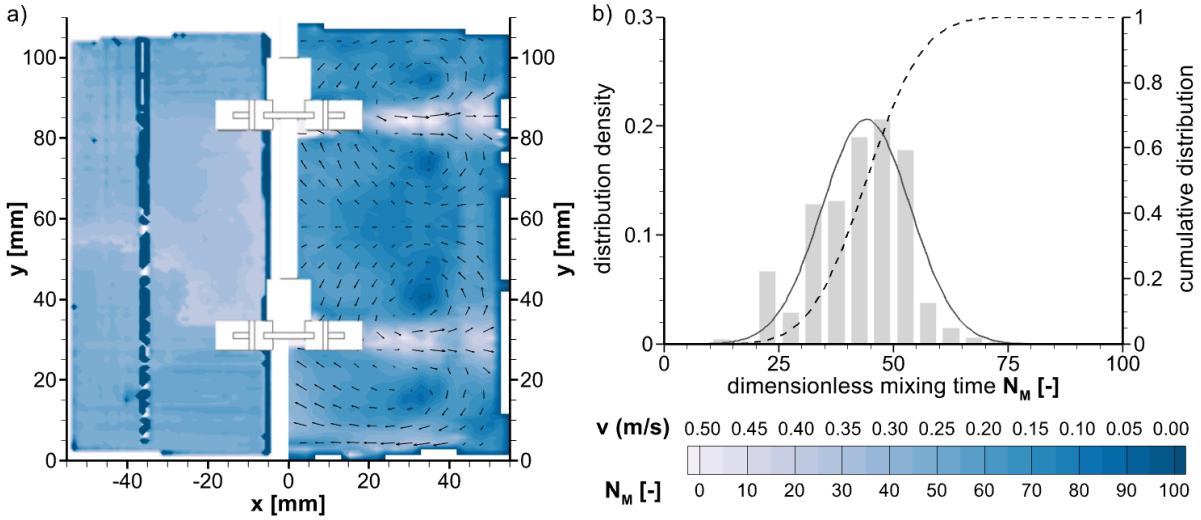

Figure 7. (**a**) MTD plot (left) and flow field (right) of the two-stage Rushton turbine, $h_1/D = 1/4$, $h_2/D = 3/4$, at $Re_R = 10{,}000$. (**b**) Distribution density (solid line) and cumulative distribution (dotted line) of the corresponding dimensionless mixing time.

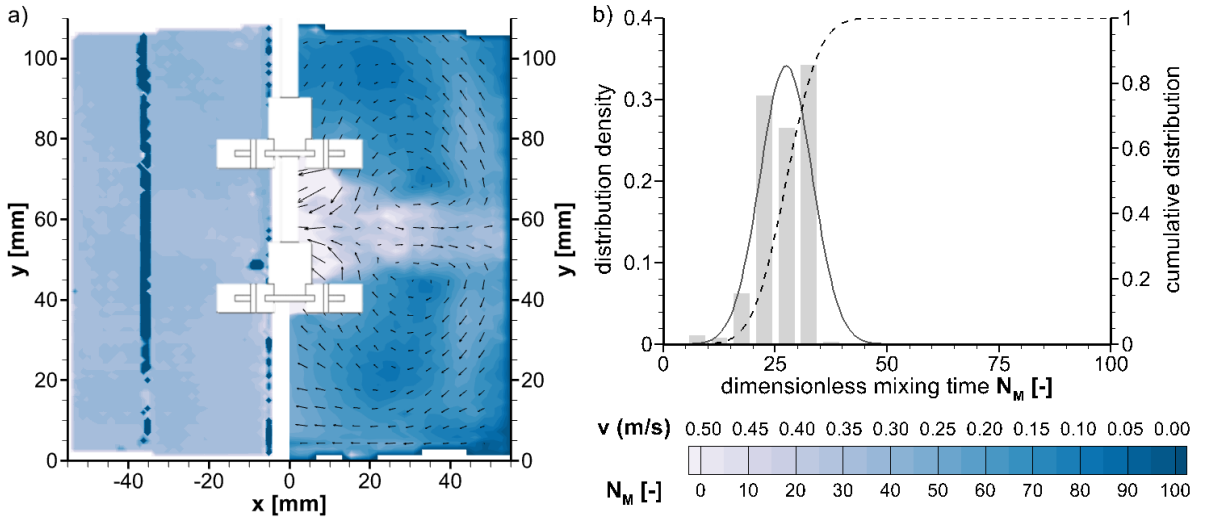

Figure 8. (**a**) MTD plot (left) and flow field (right) of the two-stage Rushton turbine, $h_1/D = 1/3$, $h_2/D = 2/3$, at $Re_R = 10{,}000$. (**b**) Distribution density (solid line) and cumulative distribution (dotted line) of the corresponding dimensionless mixing time.

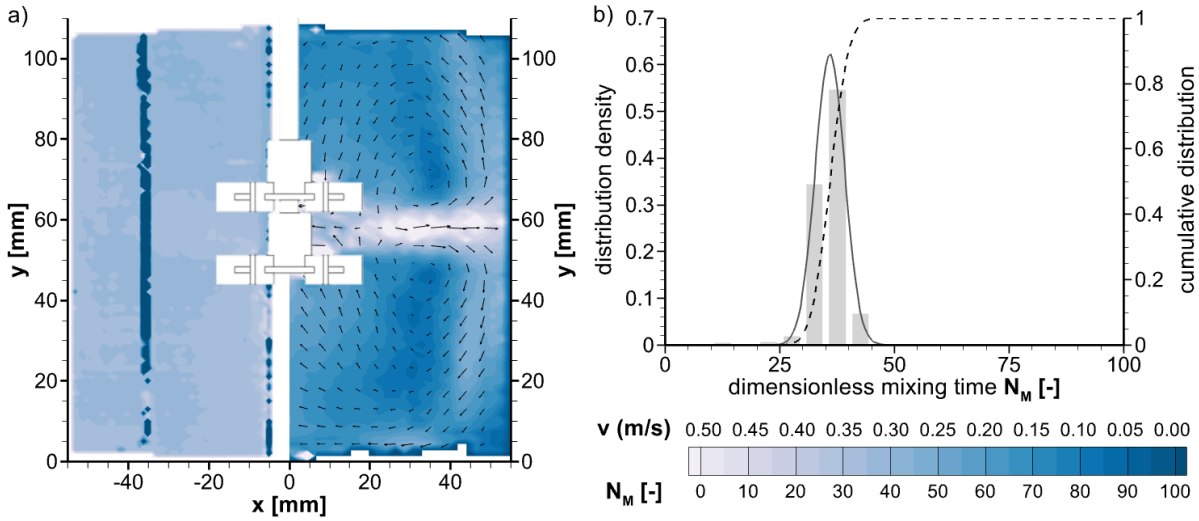

Figure 9. (**a**) MTD plot (left) and flow field (right) of the two-stage Rushton turbine, $h_1/D = 5/12$, $h_2/D = 7/12$, at $Re_R = 10{,}000$. (**b**) Distribution density (solid line) and cumulative distribution (dotted line) of the corresponding dimensionless mixing time.

Any combination of two-staged pitched blade turbines (PBTs), depicted in Figures 10–12, induces a combined, large-scale axial circulation as the primary flow field. According to Baudou et al. [39], this pattern can be observed for $\Delta h \leq 2/3$ D, which is maintained in all experiments featured in this study. Additionally, all cases display a rather homogenous mixing time distribution, with similar values as for the Rushton turbine combinations. The setup with increased distance between the two pitched blade turbine stages, with $h_1/D = 1/4$ and $h_2/D = 3/4$, is presented in Figure 10. While the large-scale, combined, axial ring vortex can be seen very clearly on the right-hand side, the left-hand side shows a largely uniform mixing time distribution over the entire reactor volume. Slightly shorter mixing times occur between the two stages, while higher values are only observed along the agitator shaft due to slight shading (due to the obvious effect of the shaft considered as a measurement artifact). Even the critical regions identified in the single-stage setup (Figure 5) close to the vessel walls and the vessel bottom, but especially just below the filling level line near the surface, are mixed quite well and show short mixing times ($\mu = 31.7$, $\sigma = 3.2$).

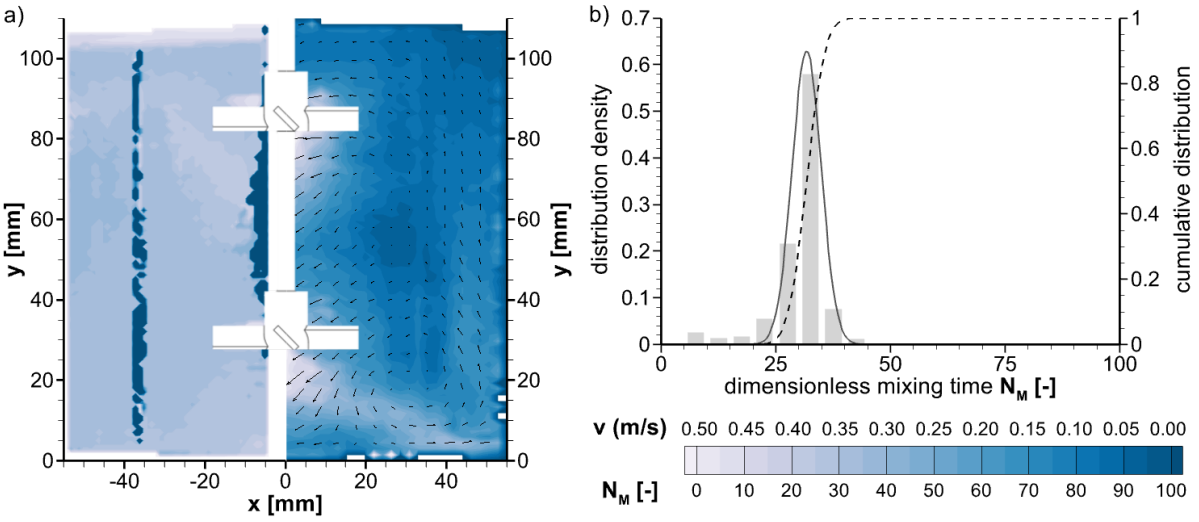

Figure 10. (**a**) MTD plot (left) and flow field (right) of the two-stage pitched blade turbine, $h_1/D = 1/4$, $h_2/D = 3/4$, at $Re_R = 10{,}000$. (**b**) Distribution density (solid line) and cumulative distribution (dotted line) of the corresponding dimensionless mixing time.

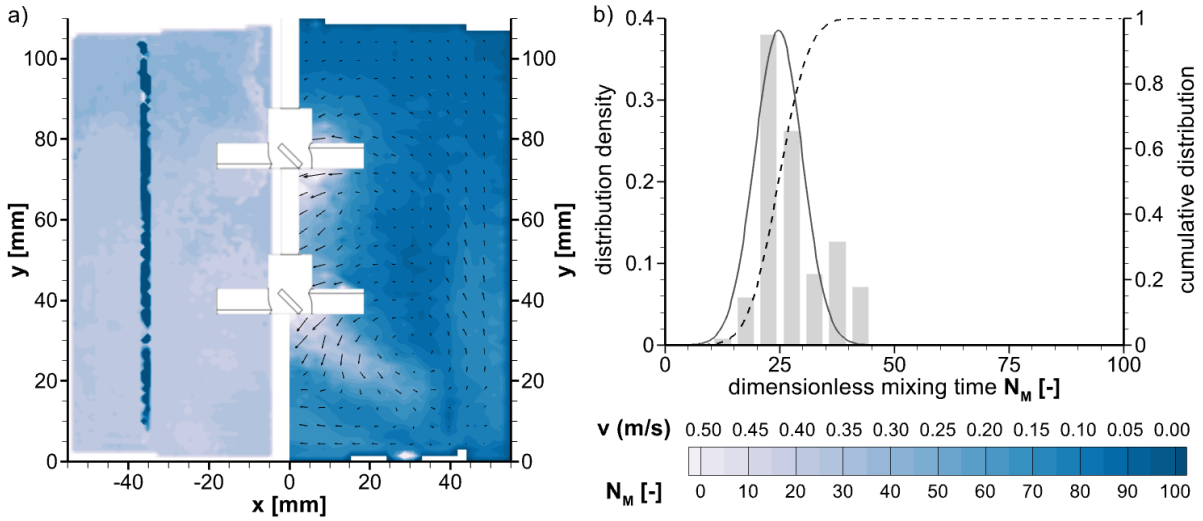

Figure 11. (**a**) MTD plot (left) and flow field (right) of the two-stage pitched blade turbine, $h_1/D = 1/3$, $h_2/D = 2/3$, at $Re_R = 10{,}000$. (**b**) Distribution density (solid line) and cumulative distribution (dotted line) of the corresponding dimensionless mixing time.

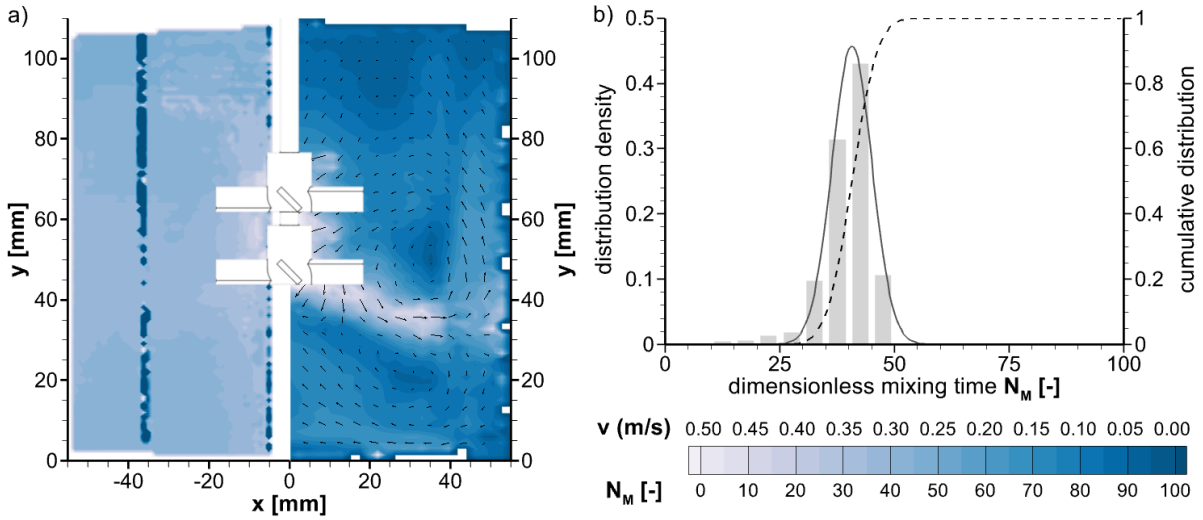

Figure 12. (**a**) MTD plot (left) and flow field (right) of the two-stage pitched blade turbine, $h_1/D = 5/12$, $h_2/D = 7/12$, at $Re_R = 10{,}000$. (**b**) Distribution density (solid line) and cumulative distribution (dotted line) of the corresponding dimensionless mixing time.

The scenario with the typical distance ($h_1/D = 1/3$, $h_2/D = 2/3$; see Figure 11) yields the shortest mean dimensionless mixing time ($\mu = 24.7$). However, the standard deviation $\sigma = 5.2$ here is higher than with the larger distance (cf. Figure 10), since the larger distance from the bottom leads to the formation of a slight dead space centrally under the lower stirrer stage. The low flow velocities and longer local mixing times in this region lead to a greater spread of the measured values.

The further decreased distance ($h_1/D = 5/12$, $h_2/D = 7/12$; see Figure 12) displays a slightly inferior mixing performance, which can be attributed to the main circulation not encompassing the entire volume in this case. In particular, the region between the upper impeller and the surface is affected by this effect. A greater upper impeller submergence leads to the formation of an increasing zone with poorer mixing and longer mixing times in the upper 35% of the volume. Consequently, the setup shown in Figure 12 shows the worst performance ($\mu = 40.7$) among the three setups featuring two-stage pitched blade turbines, as evident by the poorly mixed areas at the vessel bottom and just below the filling

level line, although the standard deviation σ = 4.4 is in the range of the typical setup (cf. Figure 11). However, for the two-stage PBTs, each of the three tested variations shows clear superiority compared to the single stage (cf. Figure 6) in terms of the mean dimensionless mixing time and the associated standard deviation.

It can be concluded that the majority of two-stage setups featured in this section, except the "parallel flow" scenario displayed in Figure 7, provide a significant improvement compared to the respective single-stage systems shown in Figures 5 and 6. This benefit of a secondary impeller in terms of shorter mixing times, a more uniform distribution of local mixing times and flow velocities is most notable in the cases involving pitched blade turbines. Among the experiments discussed in this section, the setups with standard installation heights (cf. Figures 8 and 11) prove to be preferable for effective and fast mixing. Concerning the PBTs, the one with increased distance (cf. Figure 10) seems to be acceptable, whereas the similar configuration with the RT (cf. Figure 7) exhibits even worse results compared to the single stage. The cases with decreased distance (cf. Figures 9 and 12) on the other hand do not represent any significant advantage and are therefore not recommended.

3.3. Combinations of Different Impeller Types

In this section, the impeller combinations featuring one Rushton turbine and one pitched blade turbine are presented. As discussed in a previous study [22], the setup with the Rushton turbine as the lower and the pitched blade turbine as the upper impeller induces a specific combined flow field with a radial base structure and an enlarged and intensified upper circulation. The resulting MTD plots, presented in Figures 13–15 with the same variation of impeller installation heights, indicate homogenous and fast mixing, comparable to the combinations of identical impellers presented in Section 3.2.

This impeller combination induces a unique characteristic flow pattern, with the main discharge stream of the upper axial impeller directed toward the Rushton turbine positioned beneath. From there, the fluid is distributed radially throughout the majority of the volume. In the region of the main discharge streams, slightly shorter mixing times can be identified compared to the rest of the reactor. Independently of the installation height, this impeller combination exhibits a comparatively fast mixing ($30.8 \leq \mu \leq 35.3$) with a narrow distribution of local mixing times ($2.8 \leq \sigma \leq 6.0$).

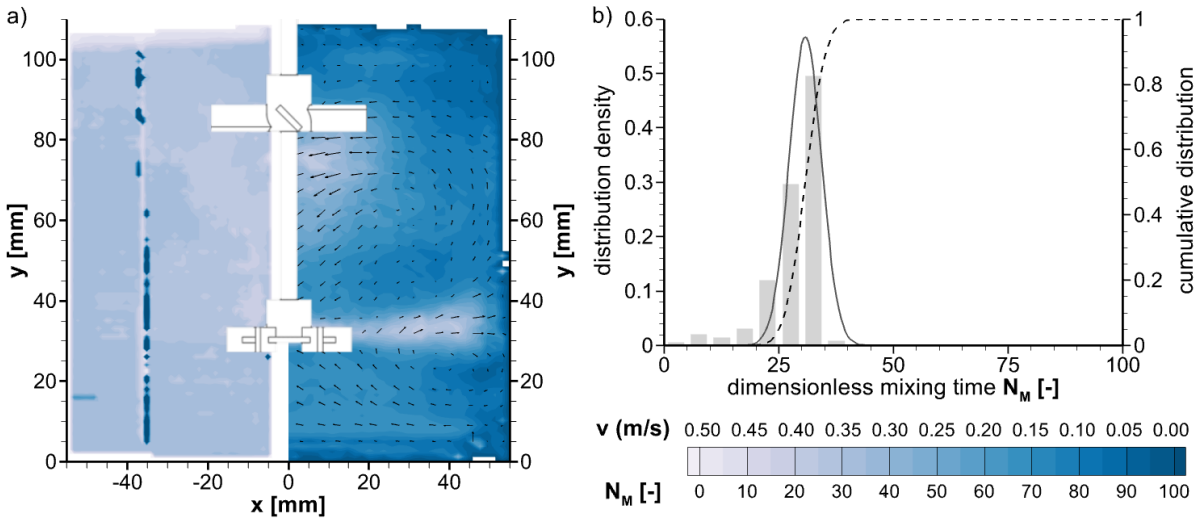

Figure 13. (**a**) MTD plot (left) and flow field (right) of the RT + PBT impeller combination, $h_1/D = 1/4$, $h_2/D = 3/4$, at Re_R = 10,000. (**b**) Distribution density (solid line) and cumulative distribution (dotted line) of the corresponding dimensionless mixing time.

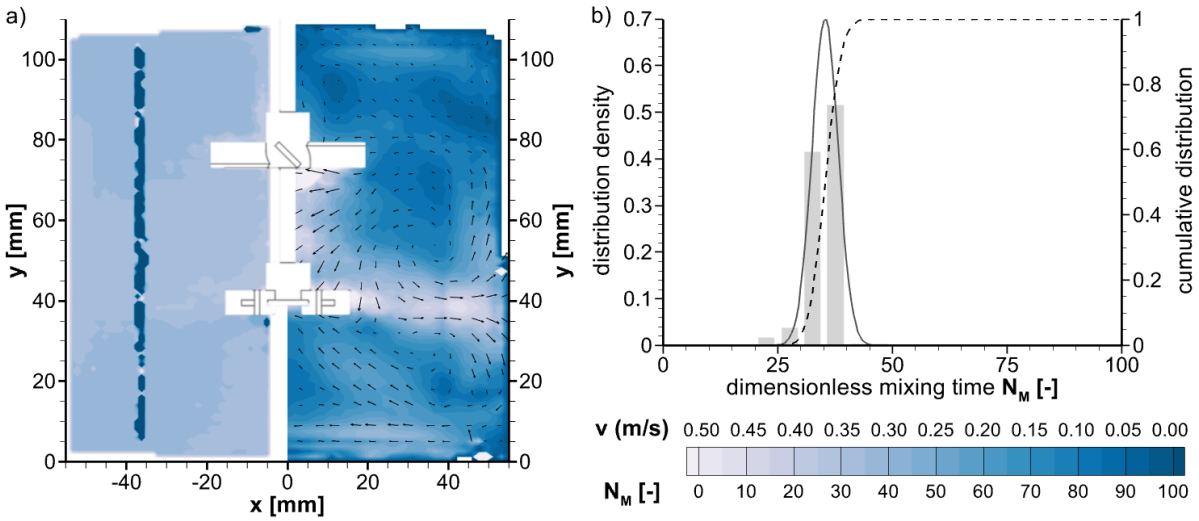

Figure 14. (**a**) MTD plot (left) and flow field (right) of the RT + PBT impeller combination, $h_1/D = 1/3$, $h_2/D = 2/3$, at $Re_R = 10{,}000$. (**b**) Distribution density (solid line) and cumulative distribution (dotted line) of the corresponding dimensionless mixing time.

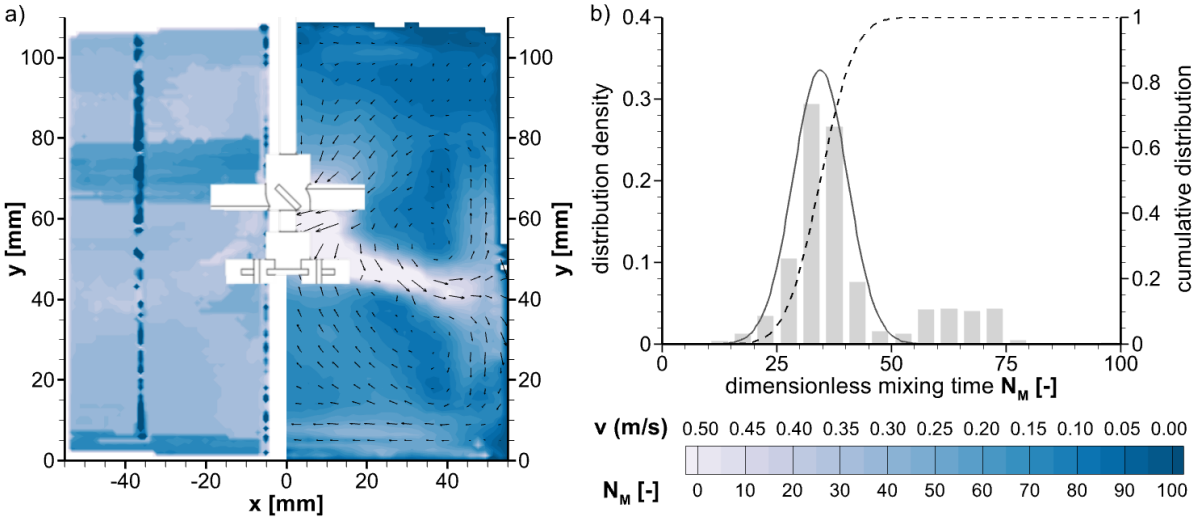

Figure 15. (**a**) MTD plot (left) and flow field (right) of the RT + PBT impeller combination, $h_1/D = 5/12$, $h_2/D = 7/12$, at $Re_R = 10{,}000$. (**b**) Distribution density (solid line) and cumulative distribution (dotted line) of the corresponding dimensionless mixing time.

The MTD contour plot of the setup with decreased distance (cf. Figure 15) contains regions with darker shading, both near the reactor bottom and slightly above the upper impeller. These, however, are measurement artifacts caused by laser light fluctuations and therefore do not represent these regions accurately. However, the central statements are not affected by this. Since the remaining, unaffected regions of this plot indicate great similarities with Figures 13 and 14, a comparable mixing pattern is most likely present. This indicates that the installation height constellation is not particularly impactful on the mixing pattern of this impeller combination. Interestingly, the large spacing configuration with a mean dimensionless mixing time of $\mu = 30.4$ (cf. Figure 13) appears to provide slight mixing time advantages. Similar to the two-stage PBTs discussed in Section 3.2, this improved state of homogenization is achieved by the closer proximity of the upper impeller toward the surface. As Figure 15 shows exemplarily, a less intensively circulated zone with higher local mixing times can form in this region, when the impellers are positioned closer toward the center of the volume.

In the second part of this section, the arrangement of the two different stirring elements is inverted. The combinations with the pitched blade at the bottom and the Rushton turbine at the top show an increased tendency of inducing flow fields with complex individual compartments. This pattern occurs even at the standard installation heights, which is distinctly unique for this combination. As a consequence, the MTD plots show a similar pattern to the two-stage Rushton turbine with increased distance (cf. Figure 7). A primary mixing zone is formed by merging back-streams at the inter-compartment boundary, which can be exemplarily seen in Figures 16 and 17. In these two experiments, the shortest mixing times are therefore found between the two stirring stages in the vicinity of the stirring shaft. Outside of this region, significantly higher values are found in the MTD plots, despite high flow velocities, especially in the respective main discharge streams of the impellers. This suggests that these setups are not particularly suitable for homogenization tasks and that turbulence and interaction of fluid elements is not ideal.

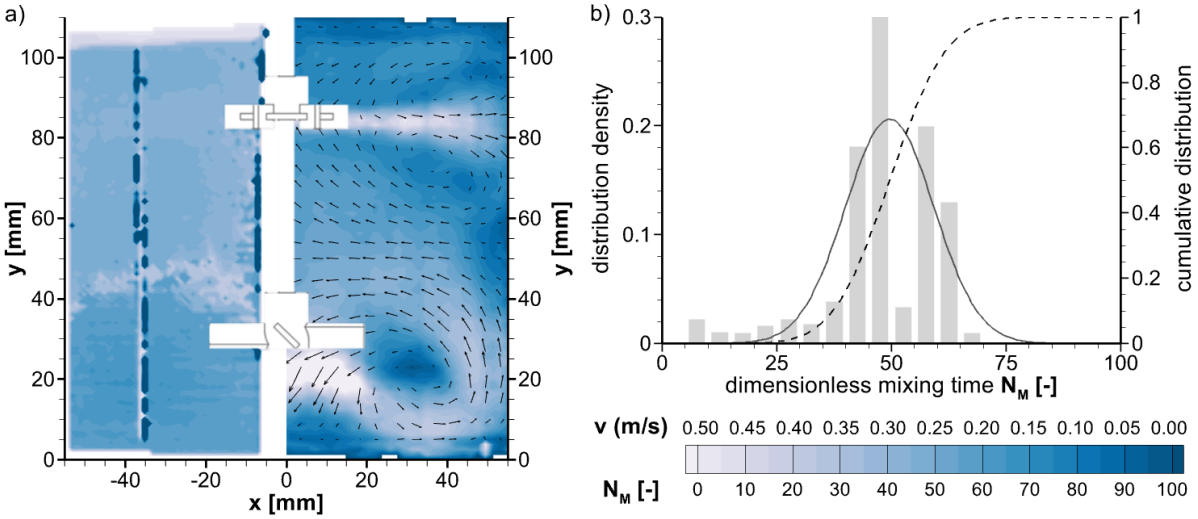

Figure 16. (**a**) MTD plot (left) and flow field (right) of the PBT + RT impeller combination, $h_1/D = 1/4$, $h_2/D = 3/4$, at $Re_R = 10{,}000$. (**b**) Distribution density (solid line) and cumulative distribution (dotted line) of the corresponding dimensionless mixing time.

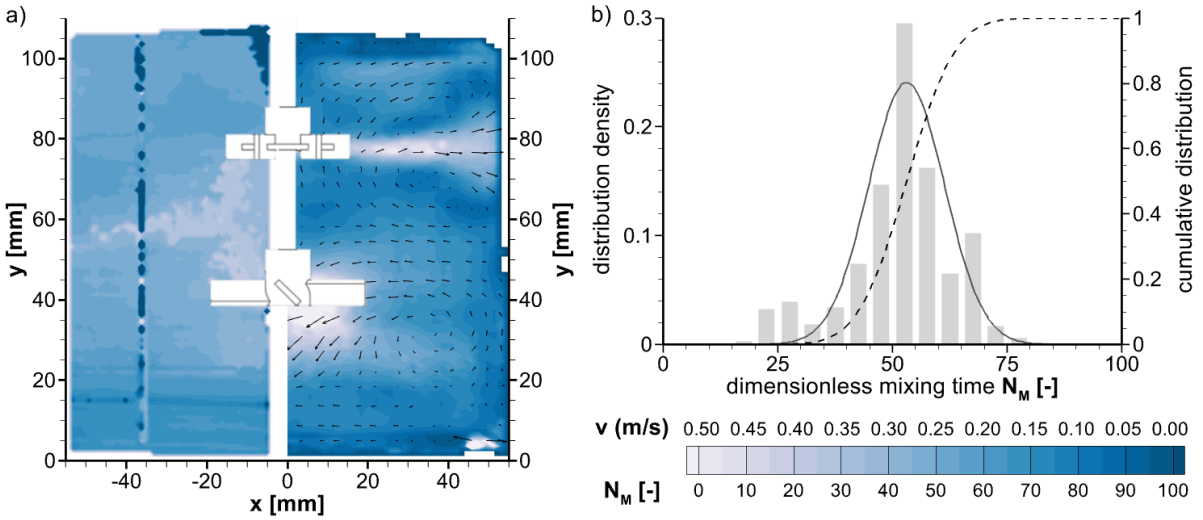

Figure 17. (**a**) MTD plot (left) and flow field (right) of the PBT + RT impeller combination, $h_1/D = 1/3$, $h_2/D = 2/3$, at $Re_R = 10{,}000$. (**b**) Distribution density (solid line) and cumulative distribution (dotted line) of the corresponding dimensionless mixing time.

The scenario with decreased distance, shown in Figure 18, induces significantly different patterns in both flow field and MTD. Here, the influence of the impeller arrangement appears to be minimal. The resulting flow field resembles that in Figure 15 much more closely than that for the other two installation heights of the PBT + RT combination (cf. Figures 16 and 17). Consequently, comparatively short and more narrowly distributed mixing times can be detected in the MTD plots, rendering this scenario the most effective variant of this impeller combination. Nevertheless, it became apparent that the PBT + RT combination performed the worst among the four investigated dual-impeller setups ($41.1 \leq \mu \leq 53.1$ and $5.0 \leq \sigma \leq 9.7$).

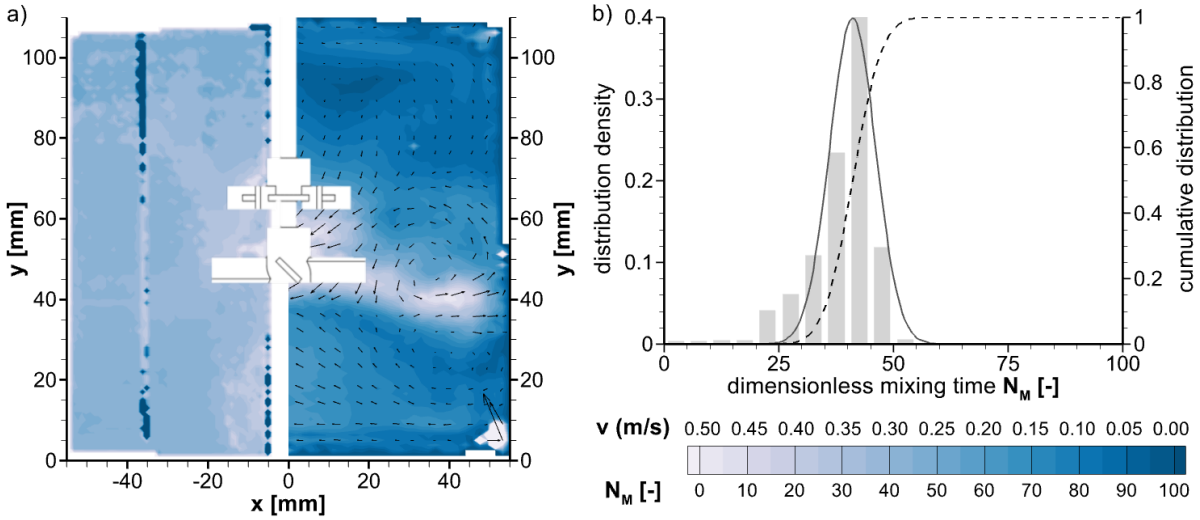

Figure 18. (**a**) MTD plot (left) and flow field (right) of the PBT + RT impeller combination, $h_1/D = 5/12$, $h_2/D = 7/12$, at $Re_R = 10{,}000$. (**b**) Distribution density (solid line) and cumulative distribution (dotted line) of the corresponding dimensionless mixing time.

3.4. Comparison of All Setups

In Table 1, the parameters of the fitted distribution functions are presented, with the lowest values of mean as well as standard deviation marked in bold. For the best homogenization process, i.e., the most rapid and uniform one, both of these parameters would need to exhibit minimal values simultaneously, which is not the case for the results of this study. The fastest average mixing time could be achieved with the two-stage PBT, followed by the two-stage RT, in both cases at the standard installation heights. Meanwhile, the RT + PBT combination yields the most homogenous MTD.

Among the two single-stage impellers, the Rushton turbine provides superior results compared to the pitched blade turbine, which was expected regarding the higher power input and flow velocity of the radial impeller. The results of the two-stage mixing experiments also show significant parallels with the flow investigations [22]. The mixing process and consequently the mixing time distribution and patterns within these matrices were proven to also be strongly dependent on the distance between the impellers and on turbulence with interacting flow regimes. Therefore, the MTD plots can be divided into two categories in analogy to the flow fields. On the one hand, scenarios with one combined flow field, such as the "merging flow" pattern, result in short mixing times with a fairly uniform distribution. On the other hand, in cases with separate flow compartments, formed by individual impellers, a primary mixing zone can be identified, where the streams merge while flowing back toward the impellers. Within these two categories, only minor differences can be found between the MTD plots of individual impeller combinations. For both the two-stage RT and two-stage PBT, the standard configuration with $h_1/D = 1/3$ and $h_2/D = 2/3$ was clearly proven to be the most efficient one among the investigated setups with different installation heights.

Among the two combinations featuring different impellers, the RT + PBT setup performs significantly superior in both metrics, which is to be expected due to the formation of combined, large-scale flow fields, in contrast to the compartments formed by the PBT + RT setup, which therefore cannot be recommended for homogenization tasks. The RT + PBT combination exhibits decent mixing results in the same order of magnitude, slightly inferior than the best scenarios of combinations of identical impellers, in all three constellations, with the increased height setup ($h_1/D = 1/4$ and $h_2/D = 3/4$) being slightly advantageous compared to the other two. In contrast to that, the PBT + RT combination does not provide an advantage over single-stage systems, with the setup with decreased distance ($h_1/D = 5/12$ and $h_2/D = 7/12$) being the only exception.

4. Discussion and Conclusions

In this study, the mixing process has been investigated in stirred tanks featuring a variety of one- and two-stage impeller setups, including combinations of identical impellers as well as setups consisting of different impellers. With the LIF technique followed by a Visual Basic evaluation of c–t curves, local mixing times could be obtained and combined into MTD plots. Despite the few systemic errors and limitations discussed in Section 2, it is possible to achieve reproductive results, as exemplarily shown in Figure 4. By directly comparing the MTD plots with the flow fields that were obtained via stereo-PIV in exactly the same geometries in previous studies [21,22], the interrelationships between flow and mixing pattern could be displayed and discussed. Additionally, a new attempt has been made to characterize the MTD mathematically via a normal distribution function. For the vast majority of measurements, this type of fit indicates a suitable representation of the data. In some scenarios with particularly narrow mixing time distribution, however, such as the RT + PBT combination at the standard heights (cf. Figure 14), the local mixing times are highly concentrated in just two of the intervals. In these cases, the normal distribution is not ideal for representation, as specifically evident by the large displacement of the derived function's peak from the experimental data.

The comparison with single-stage reference experiments shows, especially for axial conveying stirrers, that a secondary impeller stage is beneficial to accelerate the mixing process and to homogenize the MTD.

Regarding the investigated two-stage impeller setups, it can be confirmed that combined flow fields are beneficial to achieve a uniform distribution with short mixing times [35], which is not feasible in scenarios with separate flow compartments that in addition cause higher power input and therefore higher energy costs. High flow velocity on its own is not sufficient to ensure fast and homogenous mixing; the present flow patterns and local turbulence need to be taken into account as well. Regarding the combined two-stage systems, the setups with the axial stage at the top and the radial stage at the bottom showed clear advantages over the reverse variant, which had rather inconsistent flow regimes and longer mixing times. The better of the two combinations could be suitable for stirring floating particles.

The obtained results differ significantly from observations described in the literature, which can be primarily attributed to the different tracer addition method. In multi-stage impeller setups, a tracer added via the liquid surface is initially distributed in the region of the upper impeller, resulting in shorter local mixing times than around the lower impeller [41–44]. With the utilized 3D-printed injection baffle, this asymmetry can be avoided, allowing for a more uniform distribution across the liquid height as well as a more realistic representation of technical processes, where dosing usually takes place below the liquid filling line. Nevertheless, a detailed comparison of different tracer addition methods and their effect on the mixing process may be the topic of subsequent investigations. In order to assess the aspect of scale-up, measurements with a larger reactor diameter of 200 mm and a liquid volume of approx. 5 L [21] are planned as well, alongside the investigation of multiple impeller Reynolds numbers. Future studies on this topic may also include

further stirrer types [45] and a simultaneous measurement of flow fields and mixing with combined PIV/LIF systems, as, for instance, described in [46,47].

Author Contributions: Conceptualization, M.M., M.U. and H.J.S.; methodology, M.M. and H.J.S.; validation, M.M. and H.J.S.; formal analysis, M.M. and H.J.S.; investigation, M.M. and H.J.S.; resources, H.J.S.; data curation, M.M. and H.J.S.; writing—original draft preparation, M.M. and H.J.S.; writing—review and editing, M.M., M.U. and H.J.S.; visualization, M.M. and H.J.S.; supervision, M.U. and H.J.S.; project administration, M.U. and H.J.S. All authors have read and agreed to the published version of the manuscript.

Funding: This research received no external funding.

Data Availability Statement: The data presented in this study are available on request from the corresponding author.

Acknowledgments: The authors acknowledge the financial, administrative and technical support of their efforts provided by the internal research program of the University of Applied Sciences Niederrhein as well as the Institute for Coatings and Surface Chemistry (ILOC).

Conflicts of Interest: The authors declare no conflict of interest.

Abbreviations

CCD	charge-coupled device
CW	continuous wave
MTD	mixing time distribution
PIV	particle image velocimetry
LIF	laser-induced fluorescence
PBT	pitched blade turbine
RT	Rushton turbine
RIM	refractive index matching
TPU	thermoplastic polyurethane

Sub- and Superscripts

0	light/fluorescence intensity, start value
1,2	specification of an individual impeller stage, ascending from the reactor bottom
F	measured light/fluorescence intensity, start value

Symbols used

b	absorption path length	(m)
c	concentration	(g L^{-1})
d	impeller diameter	(m)
d_B	baffle width	(m)
D	tank diameter	(m)
h	impeller installation height	(m)
H	liquid filling height	(m)
I	light/fluorescence intensity	(grey levels)
K	measurement system-dependent constant	(-)
n	rotational frequency	(s^{-1})
N_M	dimensionless mixing time	(-)
Re_R	impeller Reynolds number	(-)
t	time	(s)
t_M	mixing time	(s)
x, y	horizontal and vertical coordinates	(m)
α	numerical value of the reference level of homogeneity	(-)
ε	molar extinction coefficient	(L g^{-1} m^{-1})
λ	wavelength	(m)
μ	mean	(-)
σ	standard deviation	(-)
Φ	quantum efficiency	(-)

References

1. Kraume, M. (Ed.) *Mischen und Rühren: Grundlagen und moderne Verfahren*; Wiley-VCH: Weinheim, Germany, 2003; ISBN 3-527-30709-5.
2. Zlokarnik, M. *Rührtechnik: Theorie und Praxis*; Springer: Berlin, Germany, 1999; ISBN 3-540-64639-6.
3. Crimaldi, J.P. Planar laser induced fluorescence in aqueous flows. *Exp. Fluids* **2008**, *44*, 851–863. [CrossRef]
4. Bliem, V. Untersuchung des Einflusses der Strömungsverhältnisse auf den Wärmeübergang in Rührreaktoren mit Rohrschlangeneinbauten Mittels Particle Image Velocimetry und Laser Induced Fluorescence. Ph.D. Thesis, Universität Duisburg-Essen, Essen, Germany, 2016.
5. Paul, E.L.; Atiemo-Obeng, V.A.; Kresta, S.M. (Eds.) *Handbook of Industrial Mixing: Science and Practice*; Wiley-Interscience: Hoboken, NJ, USA, 2004; ISBN 0-471-26919-0.
6. Houcine, I.; Vivier, H.; Plasari, E.; David, R.; Villermaux, J. Planar laser induced fluorescence technique for measurements of concentration fields in continuous stirred tank reactors. *Exp. Fluids* **1996**, *22*, 95–102. [CrossRef]
7. Chung, K.H.K.; Barigou, M.; Simmons, M.J.H. Reconstruction of 3-D Flow Field Inside Miniature Stirred Vessels Using a 2-D PIV Technique. *Chem. Eng. Res. Des.* **2007**, *85*, 560–567. [CrossRef]
8. Taghavi, M.; Moghaddas, J. Using PLIF/PIV techniques to investigate the reactive mixing in stirred tank reactors with Rushton and pitched blade turbines. *Chem. Eng. Res. Des.* **2019**, *151*, 190–206. [CrossRef]
9. Hu, Y.; Wang, W.; Shao, T.; Yang, J.; Cheng, Y. Visualization of reactive and non-reactive mixing processes in a stirred tank using planar laser induced fluorescence (PLIF) technique. *Chem. Eng. Res. Des.* **2012**, *90*, 524–533. [CrossRef]
10. Hu, Y.; Liu, Z.; Yang, J.; Jin, Y.; Cheng, Y. Study on the reactive mixing process in an unbaffled stirred tank using planar laser-induced fluorescence (PLIF) technique. *Chem. Eng. Sci.* **2010**, *65*, 4511–4518. [CrossRef]
11. Distelhoff, M.F.W.; Marquis, A.J. Scalar mixing in the vicinity of two disk turbines and two pitched blade impellers. *Chem. Eng. Sci.* **2000**, *55*, 1905–1920. [CrossRef]
12. Zadghaffari, R.; Moghaddas, J.S.; Revstedt, J. A mixing study in a double-Rushton stirred tank. *Comp. Chem. Eng.* **2009**, *33*, 1240–1246. [CrossRef]
13. Fall, A.; Lecoq, O.; David, R. Characterization of Mixing in a Stirred Tank by Planar Laser Induced Fluorescence (P.L.I.F.). *Chem. Eng. Res. Des.* **2001**, *79*, 876–882. [CrossRef]
14. Stefan, A.; Schultz, H.J. Use of OpenFOAM® for the Investigation of Mixing Time in Agitated Vessels with Immersed Helical Coils. In *OpenFOAM®*; Nóbrega, J.M., Jasak, H., Eds.; Springer International Publishing: Cham, Switzerland, 2019; pp. 509–520, ISBN 978-3-319-60845-7.
15. Distelhoff, M.F.W.; Marquis, A.J.; Nouri, J.M.; Whitelaw, J.H. Scalar mixing measurements in batch operated stirred tanks. *Can. J. Chem. Eng.* **1997**, *75*, 641–652. [CrossRef]
16. Wu, M.; Jurtz, N.; Hohl, L.; Kraume, M. Multi-impeller mixing performance prediction in stirred tanks using mean age theory approach. *AIChE J.* **2023**, *70*, e18247. [CrossRef]
17. Vrábel, P.; van der Lans, R.G.; Luyben, K.C.; Boon, L.; Nienow, A.W. Mixing in large-scale vessels stirred with multiple radial or radial and axial up-pumping impellers: Modelling and measurements. *Chem. Eng. Sci.* **2000**, *55*, 5881–5896. [CrossRef]
18. Machoň, V.; Jahoda, M. Liquid Homogenization in Aerated Multi-Impeller Stirred Vessel. *Chem. Eng. Technol.* **2000**, *23*, 869–876. [CrossRef]
19. Fořt, I.; Jirout, T. A study on blending characteristics of axial flow impellers. *Chem. Proc. Eng.* **2011**, *32*, 311–319. [CrossRef]
20. Matzke, M.; Behrens, C.; Jongebloed, N.; Steins, D.; Ulbricht, M.; Schultz, H.J. Investigation and Visualization of Flow Fields in Stirred Tank Reactors Using a Fluorescence Tracer Method. *Chem. Ing. Tech.* **2022**, *94*, 1131–1140. [CrossRef]
21. Jährling, K.; Schultz, H.J. Flow Fields in Stirred Vessels Depending on Different Internal Heat Exchangers and Vessel Bottoms. *Chem. Ing. Tech.* **2019**, *91*, 1281–1292. [CrossRef]
22. Matzke, M.; Ranft, E.; Dominkovic, L.; Ulbricht, M.; Schultz, H.J. Flow Field Investigations of Two-Stage Stirrer Configurations Combining Axially and Radially Conveying Turbines. *Chem. Ing. Tech.* **2023**, *95*, 1592–1602. [CrossRef]
23. Wolinski, S.; Ulbricht, M.; Schultz, H.J. Optical Measurement Method of Particle Suspension in Stirred Vessels. *Chem. Ing. Tech.* **2019**, *91*, 1326–1332. [CrossRef]
24. Radeke, L.M.; Lindner, A.; Jongebloed, N.; Ulbricht, M.; Schultz, H.J. Optimization of the Classifying Efficiency of Spiral Jet Mills by Investigating the Flow Conditions and the Grinding Performance. *Chem. Ing. Tech.* **2023**, *95*, 1603–1614. [CrossRef]
25. Jährling, K. Untersuchung von Rührprozessen mit verschiedenen Wärmetauschereinbauten und Optimierung der Strömungsregime mittels Particle Image Velocimetry (PIV). Ph.D. Thesis, Universität Duisburg-Essen, Essen, Germany, 2019.
26. Deutsches Institut für Normung. *Rührer und Stromstörer für Rührbehälter*; Beuth-Verlag: Berlin, Germany, 1992.
27. Liepe, F.; Meusel, W.; Möckel, H.O.; Platzer, B.; Weißgärber, H. Teil 4: Stoffvereinigen in fluiden Phasen: Ausrüstungen und ihre Berechnung. In *Verfahrenstechnische Berechnungsmethoden*, 1st ed.; Weiß, S., Ed.; VCH Verl.-Ges: Weinheim, Germany, 1988; ISBN 3527262059.
28. Arratia, P.E.; Muzzio, F.J. Planar Laser-Induced Fluorescence Method for Analysis of Mixing in Laminar Flows. *Ind. Eng. Chem. Res.* **2004**, *43*, 6557–6568. [CrossRef]
29. Kolano, M.; Kraume, M. Flow Compartments in Viscoelastic Fluids Using Radial Impellers in Stirred Tanks. *Chem. Eng. Technol.* **2019**, *42*, 1670–1679. [CrossRef]
30. Dantec Dynamics A/S. *Planar-LIF Software-Liquid Applications-Installation & User's Guide*; Dantec Dynamics A/S: Skovlunde, Denmark, 2002.

31. Adrian, R.J.; Westerweel, J. *Particle Image Velocimetry*; Cambridge University Press: Cambridge, UK, 2011; ISBN 978-0-521-44008-0.
32. Himmelsbach, W. (Ed.) *EKATO: The Book*, 3rd ed.; EKATO: Schopfheim, Germany, 2012; ISBN 978-3-00-037510-1.
33. Pan, C.; Min, J.; Liu, X.; Gao, Z. Investigation of Fluid Flow in a Dual Rushton Impeller Stirred Tank Using Particle Image Velocimetry. *Chin. J. Chem. Eng.* **2008**, *16*, 693–699. [CrossRef]
34. Liu, X.; Bao, Y.; Li, Z.; Gao, Z.; Smith, J.M. Particle Image Velocimetry Study of Turbulence Characteristics in a Vessel Agitated by a Dual Rushton Impeller. *Chin. J. Chem. Eng.* **2008**, *16*, 700–708. [CrossRef]
35. Rutherford, K.; Lee, K.C.; Mahmoudi, S.M.S.; Yianneskis, M. Hydrodynamic characteristics of dual Rushton impeller stirred vessels. *AIChE J.* **1996**, *42*, 332–346. [CrossRef]
36. Hudcova, V.; Machoň, V.; Nienow, A.W. Gas-liquid dispersion with dual Rushton impellers. *Biotechnol. Bioeng.* **1989**, *34*, 617–628. [CrossRef] [PubMed]
37. Fitschen, J.; Maly, M.; Rosseburg, A.; Wutz, J.; Wucherpfennig, T.; Schlüter, M. Influence of Spacing of Multiple Impellers on Power Input in an Industrial-Scale Aerated Stirred Tank Reactor. *Chem. Ing. Tech.* **2019**, *91*, 1794–1801. [CrossRef]
38. Jahoda, M.; Machoň, V. Homogenization of liquids in tanks stirred by multiple impellers. *Chem. Eng. Technol.* **1994**, *17*, 95–101. [CrossRef]
39. Baudou, C.; Xuereb, C.; Bertrand, J. 3-D hydrodynamics generated in a stirred vessel by a multiple-propeller system. *Can. J. Chem. Eng.* **1997**, *75*, 653–663. [CrossRef]
40. Armenante, P.M.; Chang, G.-M. Power Consumption in Agitated Vessels Provided with Multiple-Disk Turbines. *Ind. Eng. Chem. Res.* **1998**, *37*, 284–291. [CrossRef]
41. Fitschen, J.; Hofmann, S.; Wutz, J.; von Kameke, A.; Hoffmann, M.; Wucherpfennig, T.; Schlüter, M. Novel evaluation method to determine the local mixing time distribution in stirred tank reactors. *Chem. Eng. Sci.* **2021**, *10*, 100098. [CrossRef]
42. Weiland, C.; Salli, M.; Fitschen, J.; Hoffmann, M.; Schlüter, M. Introduction of novel characteristic time quantities to describe chemical reactors. *Chem. Eng. J. Adv.* **2023**, *16*, 100534. [CrossRef]
43. Kasat, G.R.; Pandit, A.B. Mixing Time Studies in Multiple Impeller Agitated Reactors. *Can. J. Chem. Eng.* **2004**, *82*, 892–904. [CrossRef]
44. Li, L.; Xu, B. CFD simulation of local and global mixing time in an agitated tank. *Chin. J. Mech. Eng.* **2017**, *30*, 118–126. [CrossRef]
45. Schultz, H.J. Trends und Entwicklungstendenzen in der Mischtechnik–Eindrücke und Schlaglichter der ACHEMA 2022. *Chem. Ing. Tech.* **2023**, *95*, 882–897. [CrossRef]
46. Hitimana, E.; Fox, R.O.; Hill, J.C.; Olsen, M.G. Experimental characterization of turbulent mixing performance using simultaneous stereoscopic particle image velocimetry and planar laser-induced fluorescence. *Exp. Fluids* **2019**, *60*, 28. [CrossRef]
47. Hishida, K.; Sakakibara, J. Combined planar laser-induced fluorescence-particle image velocimetry technique for velocity and temperature fields. *Exp. Fluids* **2000**, *29*, 129–140. [CrossRef]